Nuclear Instruments and Methods in Physics Research A277 (1989) 92–109
North-Holland, Amsterdam

Section III. Tracking detectors

TRACKING AT 1 TeV

H.F.-W. SADROZINSKI, A. SEIDEN and A.J. WEINSTEIN

Santa Cruz Institute for Particle Physics University of California, Santa Cruz, CA 95064, USA

We discuss the design of a tracking detector for reconstruction of charged particles in the central rapidity region at new high-energy hadron colliders such as the LHC or SSC. The physics motivation for such a tracking system is presented. Typical angles between tracks in 1 TeV jets are roughly quantified. Simple scaling rules are derived which provide a connection between the physics and detector parameters, and which can be used to evaluate the performance of different tracking devices. Based on these scaling rules and the required momentum resolution for the detector, the parameters for an all-silicon strip tracking system are defined. Estimates of the tracking efficiency are presented based on a Monte Carlo simulation of events with 1 TeV jets. Finally, the effect of spiraling tracks on detector occupancy is discussed.

1. Physics goals

Physics at new very-high energy hadron colliders will be a mixture of topics, including "bread and butter" physics such as QCD jets, physics associated with the Standard Model and its natural extensions, such as searches for the Higgs or new Z's and W's, and (hopefully) the completely unexpected. A detector for the LHC or SSC should be capable of meeting the challenges of each of these topics, and in particular should be sufficiently versatile to explore new, unforeseen phenomena. One must therefore employ a variety of detection techniques to optimize the chances of seeing and understanding these physics signals. For these reasons a sufficiently powerful tracking system will be an essential complement to calorimetry at the LHC or SSC.

In this article we outline a tracking detector design which we feel is optimized for physics at 1 TeV. Its goals are to provide full charged-particle reconstruction for TeV jets in the central region, precision secondary vertex reconstruction for high-momentum tracks (e.g. from B decays) and precision muon momentum measurement to allow detailed comparisons of rates for events with ee, $\mu\mu$ and $e\mu$ in the final state. Our approach will be to first quantify what needs to be done, tracking in the central region at the LHC or SSC. Given this, we then present a design which can meet the physics goals and which we feel is feasible to construct. Finally, we present a Monte Carlo study to evaluate the tracking efficiency and its dependence on design parameters.

Before turning to the details of the detector design, we list some of the physics goals for the tracking system.

1.1. General goals

(1) In the past, leptons have often been indicative signals for a new process. It thus seems to be natural to design a detector for the LHC or SSC to have comparable μ and e detection efficiency and momentum resolution. For particles decaying into dileptons, this will not only increase the rate by up to a factor of 4 (for example, in the case $H^0 \rightarrow Z^0Z^0$) but it will also allow a cross check of the systematics of signals of new physics and allow a determination of uncorrelated backgrounds using μe events. Good momentum resolution in a tracker also will provide the redundancy needed to reject backgrounds by comparison of the tracker momentum with the calorimeter energy for an electron, and the momentum measured in outer muon toroids for muons.

(2) For a new machine, at a very new mass scale, one would like to have the detector capabilities to look for surprises: for example, long-lived particles or jets with unusual topologies. The ability to do vertex reconstruction and to look within a jet, capabilities which calorimetry does not provide, could be critical to new discoveries.

(3) Tracking provides an important check on the calorimetry by allowing a comparison of charged and total energy observed. In addition, if tracking is done in individual time buckets, it allows a check that the relevant energy in the calorimeter comes from a single given event and not as a result of unusual event pileup.

1.2. Standard Higgs detection

Detection of the Higgs is the raison d'être of the proposed colliders, and any general-purpose detector must prove that, if the Higgs exists in the mass range dictated by the LHC or SSC energy and luminosity, it can detect it unambiguously and study its decays. Because the mass of the Higgs is not known, the detector must be multipurpose and able to search in many different channels. Precision tracking can substantially extend the mass range for a Higgs search at both the lower and upper ends and provide the momentum mea-

0168-9002/89/$03.50

Table 1
H^0 detection in a compact solenoid detector

	M_{H^0} (GeV/c²)	Signature	Advantages of Compact Solenoid Detector	Detected Rates Per Year (10^{40} cm^{-2})
Intermediate Higgs	60	$H^0 \to \gamma\gamma$	· Good π^0/γ separation in microconverter	500
	100	H^0W with $W \to \ell\nu$, $H^0 \to b\bar{b}$	· Vertex detection (b tag) · Good μ/e ID in Jets · Good missing P_T	400
	150	$H^0 \to ZZ^*$	· Good Z mass reconstruction in both $\mu\mu$ and ee	
	$2M_Z$			
	300			140 ($Z \to e$ only) 560 ($Z \to \mu, e$)
		$H^0 \to ZZ \to 4\ell^{\pm}$ $\to ZZ \to \ell^+\ell^-\nu\bar{\nu}$ $\to WW \to \ell\nu\ell\nu$	· Good Z mass measurement in both ee and $\mu\mu$ up 1 TeV · Good missing P_T	
Heavy Higgs	500			29 ($Z \to e$ only) 116 ($Z \to \mu, e$)
		$H^0 \to WW$ with $W \to e\nu, \mu\nu, \tau\nu$, $W \to q\bar{q}$	· Best jet capability: · Calorimetry	5000
	700	$\to ZZ$ with $Z \to \ell^+\ell^-$, $Z \to q\bar{q}$	· Precise, hi resolution analysis of charged tracks and neutrals inside jets	1000
	1 TeV	$W^{\pm}W^{\pm}$	· Precise lepton measurement in TeV range	

surement for full use of muons and electrons in the intermediate mass range.

The main diagrams of interest for the production of the Higgs are shown in fig. 1. The Higgs decay will vary depending on its mass. This breaks up into two regimes, the regime with $m_H < 2m_W$, where the decay is mostly into heavy quark or lepton pairs, and $m_H > 2m_W$, where the decay is primarily into gauge boson pairs. In this upper mass range the energy and luminosity of the machine will dictate if enough events are available in all lepton final states, originating from the gauge boson decay, or if hadronic decays must be used. We will therefore discuss three regimes below, which we call the light, intermediate and heavy Higgs cases. Relevant event rates used below and summarized in table 1 come from the recent Report of the Compact Detector Subgroup [1] at the 1987 Workshop at Berkeley on detectors at the SSC and are based on the work of a large number of participants at that meeting.

1.2.1. Light Higgs

At the time the LHC or SSC will start physics, existing machines would have found the Higgs if its mass is less than about 85 GeV. Since the top quark appears to be quite heavy, it is likely that a light Higgs of mass $\lesssim 2m_W$ would decay predominantly into $b\bar{b}$ quarks. To improve the experimental signature it will be essential to look for the associated production of the H^0 decaying into $b\bar{b}$ with a W, as in fig. 1a. The detection of the $b\bar{b}$ pairs will rely on the ability to reconstruct detached vertices efficiently. Note that only a few percent of the moderate-P_T jets relevant here contain a

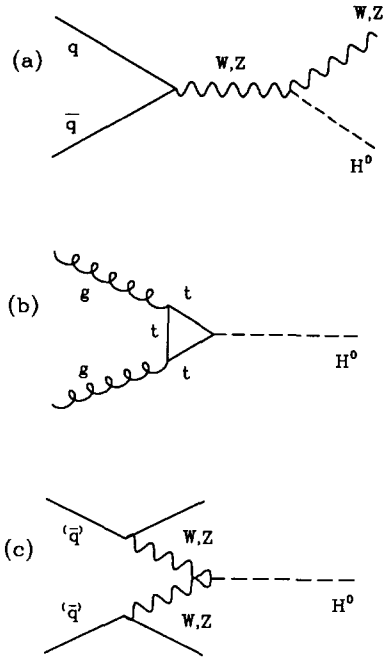

Fig. 1. Diagrams for H^0 production in pp collisions.

b-quark [2], and thus tagging the two B-mesons from the Higgs decay will reduce the background from low-P_T jets by a factor of over 100.

The process ($pp \rightarrow W + H^0$, $H^0 \rightarrow b\bar{b}$) has been discussed in ref. [3]. In this study the transverse momentum in the fundamental parton scattering is chosen to exceed 50 GeV and the W and one B-meson are required to decay into leptons by the trigger. Both jets from the H^0 have to have decay vertices with impact distances in the transverse plane of ≥ 50 μm. It is significant that the surviving background events contain largely pairs of b quarks. In one year of running SSC one expects, for an H^0 mass of 100 GeV, about 400 signal events over a background of 2100 from gg and $q\bar{q}$ production, which is an 8-standard-deviation effect. These numbers are for a mass window 20 GeV wide and could, perhaps, be improved if better mass resolution could be obtained. The ability to see vertices at the level that permits this 50 μm cut is crucial, as without the vertex cuts the signal represents a much less significant excess over the background (about 700 events over a background of 54000) [4].

We have studied the process ($pp \rightarrow W + H^0$, $H^0 \rightarrow b\bar{b}$), using PYTHIA 4.8 [7]. After tagging on the high-P_T lepton and missing energy from the W decay, we have studied the distribution of impact parameters for tracks in the jets versus the Feynman track $x_F \equiv P \cdot P_{jet}/P_{jet}^2$. Tracks from the decay of the leading long-lived B-meson in the b-jet should have large x_F. As discussed below, we use an impact parameter resolution, dominated by multiple scattering, of 80 μm/P. If we require at least two tracks in the jet to have $x_F > 0.05$ and impact parameter > 50 μm, we identify b-jets from Higgs-decays with an efficiency of $\simeq 40\%$. When we require two such jets, the dominant background due to a (W + QCD) jet is rejected by a factor of 100.

1.2.2. Intermediate-mass Higgs

In the clean heavy Higgs channels like ($H \rightarrow ZZ$, $Z \rightarrow l^+l^-$) we will be rate-limited, and detector optimization is important. If we restrict ourselves to electrons only, a Higgs with a mass of 300 GeV will yield 140 events per SSC year; this drops to 29 events for a 500 GeV Higgs. If the momentum resolution is good enough to allow the use of muons as well, these rates are increased by a factor of 4. Additionally, combinatorial backgrounds (for example, from the heavy top) can be measured in μe channels and like-sign channels.

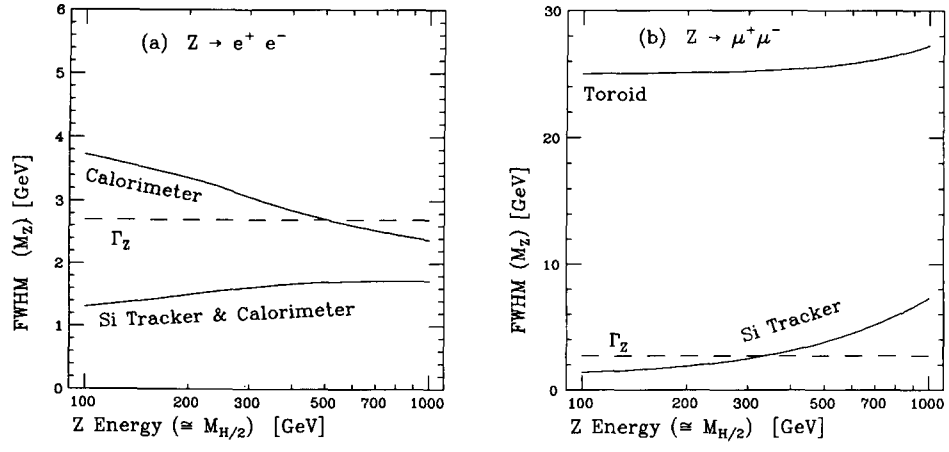

Fig. 2. FWHM resolution of the Z^0 mass as a function of Z^0 energy for a detector with calorimetry only, and for a detector including precision Si tracking. (a) $Z^0 \rightarrow e^+e^-$; (b) $Z^0 \rightarrow \mu^+\mu^-$.

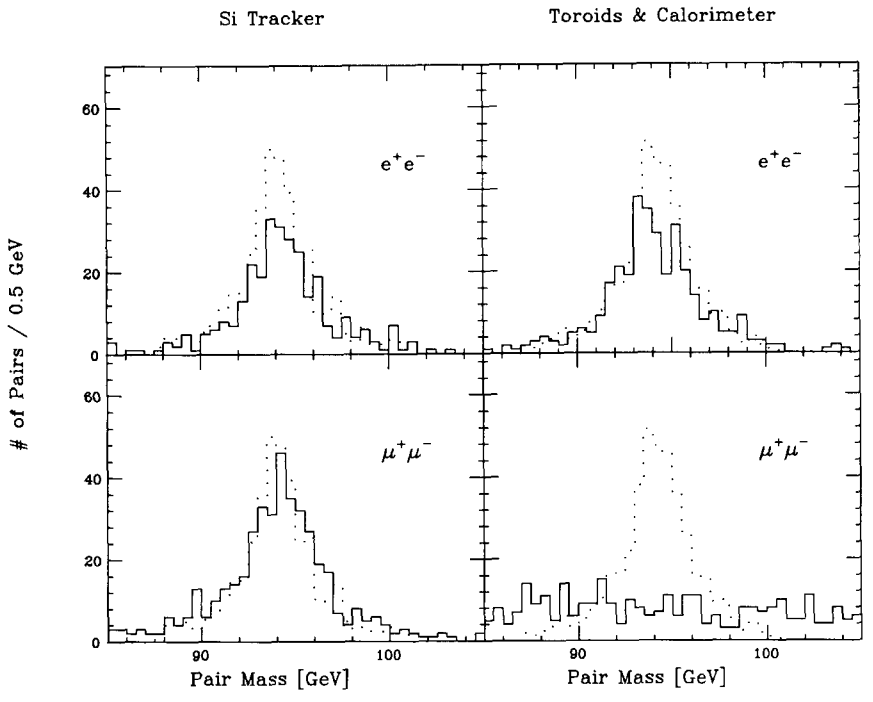

Fig. 3. Reconstructed Z^0 invariant mass from a 500 GeV Higgs decay, using e pairs and μ pairs, from the proposed precision Si tracker or a calorimeter with muon toroids only. The detector resolution yields the histogram, to be compared with perfect resolution (dotted line).

A figure of merit to quantify the needed momentum resolution is the mass resolution for reconstructed Z^0, which should be less than the natural width, $\Gamma_Z/2.35$. This should be true over as large a range as possible, and certainly up to a Higgs mass of at least 500 GeV where rates for all lepton final states are adequate. We can estimate that this requires $\sigma_{P_T}/P_T \leq 2\%$ at about 200 GeV. We will look at the mass resolution given by the silicon strip detector discussed later in the text. The single-track momentum resolution is shown in fig. 23. Our results here provide the main motivation for the choice of magnetic field and outer radius for the tracking detector.

We have generated, using ISAJET [5], the process $pp \rightarrow H^0 \rightarrow Z^0Z^0$, with each $Z^0 \rightarrow l^+l^-$, varying the mass of the Higgs from 200 GeV to 2 TeV. Leptons are kept if their $P_T > 10$ GeV and the magnitude of their rapidity < 2.5. The invariant mass of each Z^0 is calcu-

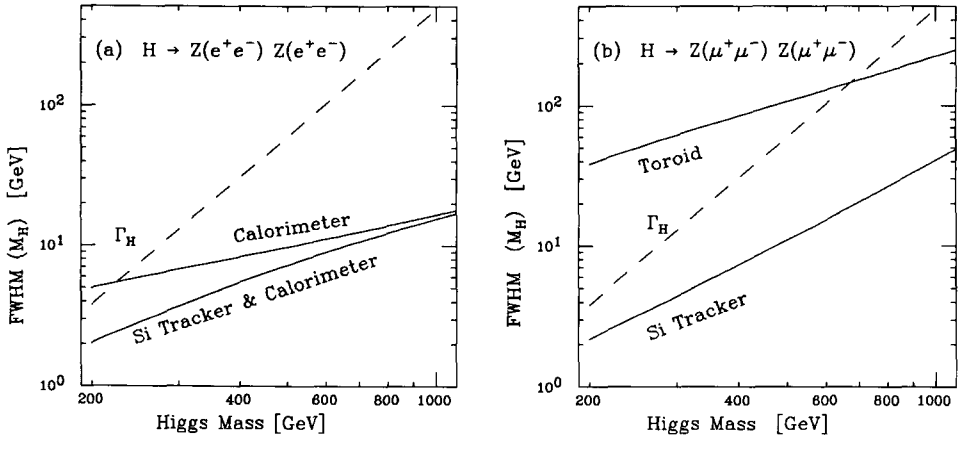

Fig. 4. Z^0Z^0 invariant-mass resolution for different detector configurations, compared with the expected Higgs width Γ_H (dotted line). (a) $Z^0 \rightarrow e^+e^-$; (b) $Z^0 \rightarrow \mu^+\mu^-$.

lated after momenta are smeared. Fig. 2 shows the FWHM resolution of the Z^0 mass as a function of the Z^0 energy ($\sim m_{H^0/2}$) for e or μ pairs, respectively. Results are given for a detector with calorimetry and muon toroids only and for one with precision silicon tracking as well. We also indicate on the figures the natural Z^0 width. We can conclude that with precision tracking we can reconstruct Z^0's from H^0 with a resolution comparable or better than the Z^0 width, up to Higgs masses of nearly 1 TeV. In fig. 3, we show the Z^0 invariant mass plot for a Higgs mass of 500 GeV and compare it with the case of perfect resolution (dotted line) which is governed by the natural width of the Z^0. The resolution for the case of precision tracking shows little deviation from the Z^0 width, but for a toroidal μ tracker alone the signal is completely smeared out.

Finally, in fig. 4 we show the resolution in the Higgs mass itself using the $Z^0 \to l^+l^-$ channels and comparing with the expected Higgs width Γ_H. With precision tracking the resolution is below Γ_H even for low Higgs masses.

1.2.3. Heavy Higgs

For Higgs masses close to 1 TeV, one of the W's or Z's in the Higgs decay has to be detected in its hadronic mode to have enough events in one SSC year. As pointed out by Protopopescu [6], the background from W + jet, where the mass of the jet is close to the W mass, is so large that the signal-to-background ratio is 360/2800 when only calorimetry is used. Further cuts using calorimetry can improve this ratio considerably at the expense of loss of signal. In either case, precision tracking inside the jet will provide additional discrimination between W jets and quark/gluon jets by using the difference in the jet structure. Note that a 1 TeV W still decays into an average of about 18 charged particles, like a W at rest, while a 1 TeV QCD jet system with invariant mass accidentally near m_W will usually fragment into many more particles.

To check these ideas, we generated, using PYTHIA 4.8, either Higgs → WW or a W-jet system, both with invariant mass of 1 TeV. We selected events containing a high-P_T lepton and a jet with invariant mass near that of the W. We then counted the number of charged tracks with $P_T > 1$ GeV in the event. In fig. 5 we show the distribution of the charged multiplicity N_{ch} in (a) W + jet events ($\bar{N}_{ch} = 62$) and (b) W + W events ($\bar{N}_{ch} = 29$). A cut at $m < 35$ leaves 78% of the W + W events while cutting out 86% of the W + jet events. The ability to use the tracking information in the core of the jets is increasing the signal-to-background ratio in the above example by a factor of 5.6, making a difficult measurement feasible.

We consider the above analysis to be only a first step in what can be done using tracking to distinguish high-energy but "stable light parent" jets from QCD jets.

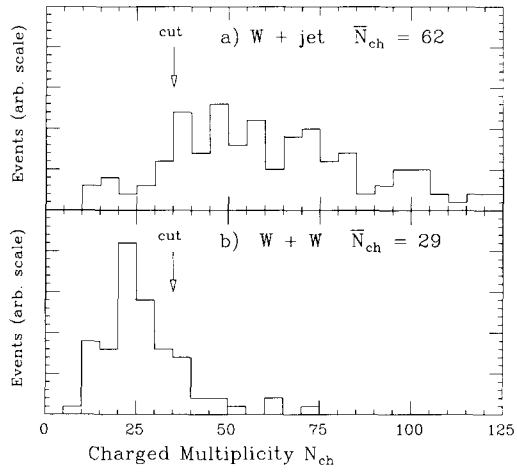

Fig. 5. Charged multiplicity in (a) W + jet events and (b) W + W events, with cuts as described in the text.

Other useful quantities after the multiplicity cut might be the fraction of charged and neutral energy, the fractional momentum of the fastest charged particle in the jet and the presence of secondary jets within the high-energy jet. In addition it will be important to understand how these quantities depend on the fragmentation model chosen. The independent fragmentation scheme employed by ISAJET produces quark and gluon jets with significantly higher multiplicity ($\bar{N}_{ch} = 47$ for a 500 GeV quark/gluon jet) than those produced with the LUND parton shower model scheme employed by PYTHIA ($\bar{N}_{ch} = 30$). Results presented in this work use the more conservative of the two Monte Carlos, as appropriate.

2. Requirements for a tracking system

To reconstruct leading particles in the core of jets will require a system which can resolve very closely spaced particle trajectories. In order to quantify this problem, prior to a sophisticated Monte Carlo simulation, we will try to define a mean track separation angle $\langle\theta\rangle$, at production, which characterizes the leading particles in a jet. In general these particles will have a momentum $\gg 1$ GeV.

We look first at simulations of 1 TeV gluon and quark jets using QCD evolution models such as ISAJET or PYTHIA. Fig. 6 shows the expected mean multiplicity for gluon and quark jets from PYTHIA. At 1 TeV, gluon jets are expected to have about 70 charged particles, quark jets about 40 [9].

Fig. 7 shows the energy dependence of $\theta_{1/2}$ for gluon and quark jets, where $\theta_{1/2}$ is the angle relative to the jet direction at which the energy flow drops by a factor of 2 [9]. At 1 TeV: $\theta_{1/2} \simeq 20$ mrad for gluon jets,

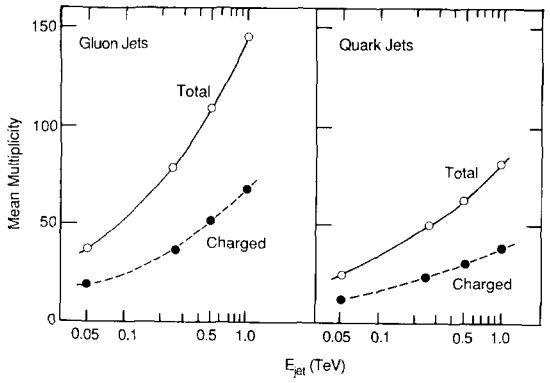

Fig. 6. Mean multiplicity versus jet energy for jets initiated by gluons or light quarks.

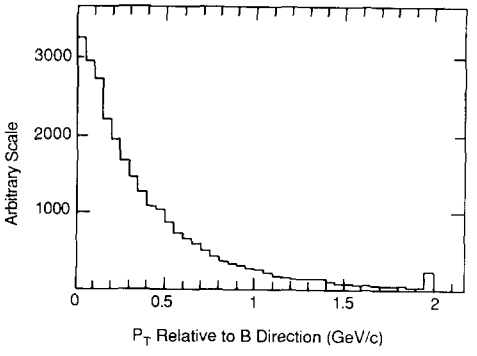

Fig. 8. P_T of charged tracks from B meson decay, relative to B direction.

and $\theta_{1/2} \simeq 4$ mrad for quark jets. Since a jet contains many particles, $\langle\theta\rangle$ is expected to be about an order of magnitude smaller than $\theta_{1/2}$. Thus, a goal for a tracking system would be to be able to resolve particles produced at angles to each other of $\langle\theta\rangle \simeq 0.5$ mrad. We will arrive at this number in another way below. Note that this implies that a two-hit segmentation of 500 μm is required at a radius of 1 m, which is very difficult for conventional drift chambers. Even a silicon strip tracking system could not fully resolve all the particles until a radius $\gtrsim 20$ cm, assuming a double-track resolution of 100 μm.

As an alternative method to arrive at $\langle\theta\rangle$, we can use the extensive Monte Carlo work on B tagging at the Z^0 [10]. Fig. 8 shows the transverse momentum of particles from B decays. A typical value is about 500 MeV, rather similar to light quark jets at the same energy scale. Fig. 9 shows the fraction of B's that can be reconstructed at the Z^0 using a tracking system with resolving angle $\Delta\phi$ between neighboring tracks and requiring that at least three charged secondaries are reconstructed. To achieve $> 90\%$ efficiency requires $\Delta\phi = 5$ mrad. Scaling each jet up to 1 TeV (a factor of 20) would give us a requirement of $\Delta\phi \simeq 0.25$ mrad for B reconstruction. Thus, a choice of $\langle\theta\rangle = 0.5$ mrad to characterize neighboring particles in the jet core is a reasonable choice.

Using a typical P_T of 500 MeV we can estimate a minimum momentum, P_{min} of particles in the core of a jet as 500 MeV/$\theta_{1/2}$. Using $\theta_{1/2} \sim 10$ mrad gives $P_{min} = 50$ GeV for a 1 TeV jet. Thus, a tracking system will need a resolving power $\sim \langle\theta\rangle$ for tracks with $P \gtrsim P_{min}$, but can reconstruct particles with $P \ll P_{min}$ with a poorer segmentation since these are typically outside the core of the jet.

We have totally ignored the magnetic field in the above discussion. As long as tracks with $P > P_{min}$ are bent by an angle $< \theta_{1/2}$, the presence of a magnetic field does not significantly help the track reconstruction problem. For $P_{min} = 50$ GeV, $\theta_{1/2} = 10$ mrad, the magnetic field does not help substantially for reasonable choices for the field and tracker radius.

3. Design of a 1 TeV tracking system

Because of the very fine segmentation needed to resolve tracks, a tracker will probably have to use infrequent sampling to avoid ending up with an enor-

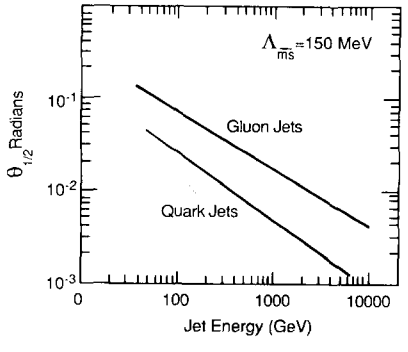

Fig. 7. Energy dependence of the angle at which the energy flow drops by a factor of 2.

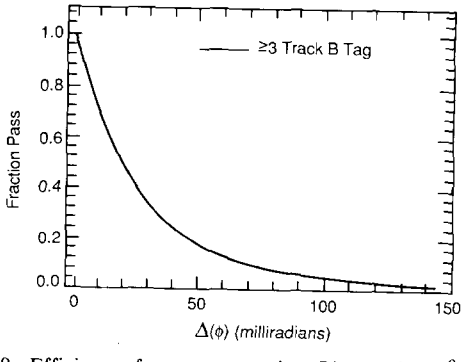

Fig. 9. Efficiency for reconstructing B's at the Z^0 versus angular resolving power of the tracking system.

mous number of channels. It will, in addition, have to go out to a moderately large radius since it is critical not only to resolve tracks, but also to measure their momentum.

A model for the organization of such detectors is the vector tracking chamber, made of jet cells. The jet cell geometry was introduced by the JADE collaboration. The first of such chambers incorporating stereo wires, and smaller jet cells to aid in pattern recognition, was used by the Mark III detector. Subsequent examples are the trackers for the Mark II, CDF, SLD and ZEUS. The vector tracking ideas work equally well for other detector elements, appropriately organized. We will look in some detail at the organization of a tracker made entirely of silicon strips. The silicon strips are very attractive since they offer extremely good resolution in space and time. In addition, it is an area where much progress is being made and the detectors, for the scale discussed below, are still affordable in price. We feel this solution is well matched to tracking at 1 TeV. Note also that the use of a vector tracking chamber allows a crude local calculation of the transverse momentum, using track segments, allowing the reconstruction of high transverse momentum tracks only, in a efficient manner. This would vastly shrink the computer time needed for track reconstruction for events in which only high-P_T tracks are desired.

3.1. Tracker parameters

The parameters of the tracker are as follows.

(1) It is made of 16 layers of silicon strips (25 μm pitch) organized into 8 pairs (superlayers) of detectors. The detectors are assumed to be double-sided (one side axial and one side stereo), so the total number of measurements is 32. Thus, the detector can be thought of as 8 axial and 8 stereo superlayers, although the axial and stereo measurements occur grouped together locally. This can be compared to typical vector drift chambers, such as the new Mark II chamber, which has 6 superlayers of each type.

(2) The radius varies from 8 to 50 cm. The inner radius is determined by the amount of radiation damage that can be tolerated. For the SSC operating at a luminosity of 10^{33} cm^{-2}s^{-1} this inner radius corresponds to about 0.4 Mrad per year [11]. Clearly, the design of sufficiently radiation-resistant electronics is critically important. Note that for high-momentum tracks the impact parameter error is still ~ 5 μm, even starting 8 cm from the origin, since the long lever arm of the tracking device provides a very well measured angle and curvature.

(3) We assume each layer is 150 μm thick and has double-sided readout. This gives 2.5% of an X_0 of material for the silicon and probably about 4 to 5% of an X_0 in total if we include a support structure. It is of great importance to maintain the amount of material in this range to avoid creating many soft electron–positron pairs from photon conversions (see chapter 5). In addition, B vertex reconstruction for the light-Higgs scenario involves lower-momentum tracks and is sensitive to multiple-scattering errors. For our design the multiple-scattering contribution to the impact parameter error is about 80 μm/P [GeV]. If we require an error $\lesssim 20$ μm, this implies B tagging with tracks with $P > 4$ GeV. For the light-Higgs search discussed above we find that the efficiency for reconstructing a 100 GeV Higgs $\rightarrow b\bar{b}$, with at least two charged tracks falling within the central ± 2 units of rapidity, is reduced by only 14% if we require B tagging with two tracks > 4 GeV.

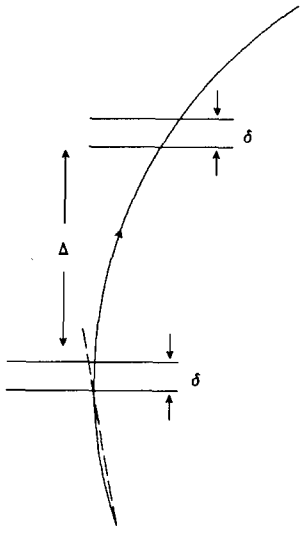

Fig. 10. A track passing through two adjacent layer pairs.

3.2. Pattern recognition requirements

In fig. 10 we show two pairs of detector layers. The detector arrangement is specified by the distances δ and Δ, which specify the separation between pairs in a superlayers, respectively. The conflicting demands on δ and Δ are follows.

(a) We would like δ small enough to make matching of points on a track simple.
(b) We would like δ large enough so that the track angle (tangent vector) is well measured.
(c) We would like Δ large enough to fill a given space.
(d) We would like Δ small enough to allow frequent sampling

The basis for linking vector segments is shown in fig. 11 [12]. The angle between the tangent vectors and a chord connecting the segments is the same for both vector segments belonging to the same circle.

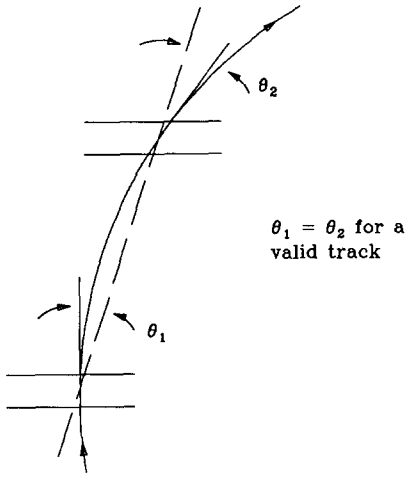

Fig. 11. Relation for vector segments lying on one track.

For the pattern recognition we require that:
(1) different tracks give distinct hits,
(2) hits in the paired layers, separated by δ, can be locally associated into correct vector segments, and
(3) vector segments from different pairs can be correctly linked into tracks.

In terms of the angular track separation characterizing the physics and the tracker parameters we demand that the tracker provides the resolution for the three steps above which have distinctly different requirements. We define:

ρ_{track} = track's radius of curvature;
$\langle\theta\rangle$ = typical track separation angle;
σ_m = position resolution of measuring element;
ϵ_m = two-track resolving power in space, locally, for a measuring element;
δ = separation of elements used to measure track vectors;
r_m = outer radius of device;
r_i = mean radius of the ith pair.

From the physics considerations discussed earlier, $\langle\theta\rangle \simeq 0.5$ mrad. For a silicon strip detector with 25 μm pitch, $\sigma_m \simeq 5$ μm and $\epsilon_m \simeq 100$ μm. Suitable signal processing could distinguish tracks entering adjacent microstrips, giving $\epsilon_m \simeq 25$ μm at the expense of a slightly degraded position resolution.

3.2.1. Satisfying pattern recognition requirements

We now quantify the relation between parameters so that the three pattern recognition requirements can be met.

(1) To see distinct hits from different tracks in layer i we need $\epsilon_m < r_i\langle\theta\rangle$. How many layers do we need? We can expect that we need at least three at radii greater than $r = \epsilon_m/\langle\theta\rangle = 100$ μm/0.5 mrad = 20 cm. Thus, taking 8 pairs with 8 cm $\leq r_i \leq$ 50 cm gives 5 pairs at radii $r_i \geq 20$ cm and 4 pairs at $r_i \geq 29$ cm, which is the mean radius. Thus, the device should be able to yield a sufficient number of distinct hits for nearly all of the tracks.

(2) To match points into a segment we choose the simplest algorithm illustrated by the dashed line in fig. 10. To each point in the inner layer of a pair we associate the point with the most similar ϕ angle in the outer member of the pair. For a curving track the deviation in space from a perfect match, using this algorithm, is given by $[r_i/(2\rho_{\text{track}})]\delta$. However, in the jet core we can expect nearby hits from very stiff tracks with a mean spacing of $\langle\theta\rangle r_i$. These can cause incorrect associations in segment formation. Thus, the simple algorithm for matching points into vectored segments will work provided:

$$\frac{r_i}{2\rho_{\text{track}}}\delta < \langle\theta\rangle r_i,$$

or

$$\frac{\delta}{2\langle\theta\rangle} \lesssim \rho_{\text{track}}.$$

This relation needs to be valid for all momenta within the jet core and provides the motivation for a small δ. Taking, for example, $\delta = 1$ cm we get easy association into vectors for $\rho_{\text{track}} \gtrsim 1$ cm/(2 × 0.5 mrad) = 10 m.

This corresponds to 10 GeV at 3.3 T. It is substantially below the P_{min} of 50 GeV for tracks in the jet core estimated above. Note, that the deviation from a perfect straight line match of the points to be associated is only 100 μm at a radius of 20 cm for $\rho_{\text{track}} = 10$ m. The matching of pairs within a segment is the one relation sensitive to the B-field and would argue for the smallest field, although, as seen above, a value close to 3 T should work.

(3) The basis for linking vector segments is illustrated in fig. 11. Each angle θ_1 or θ_2 is measured

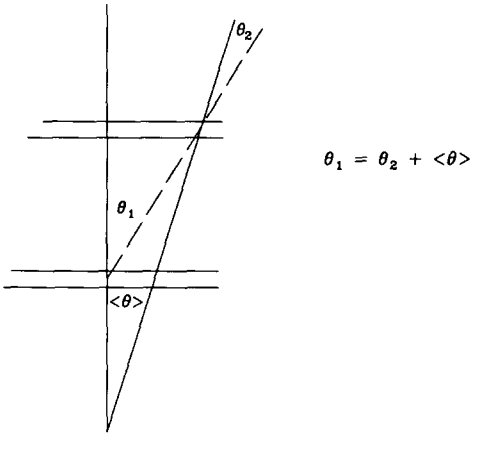

Fig. 12. Angular relations for a spurious track (dashed) created from hits from two real tracks.

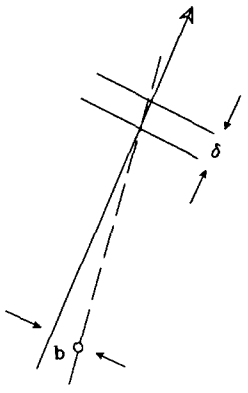

Fig. 13. Relation of points to be associated into a vector segment for a stiff track with impact parameter b.

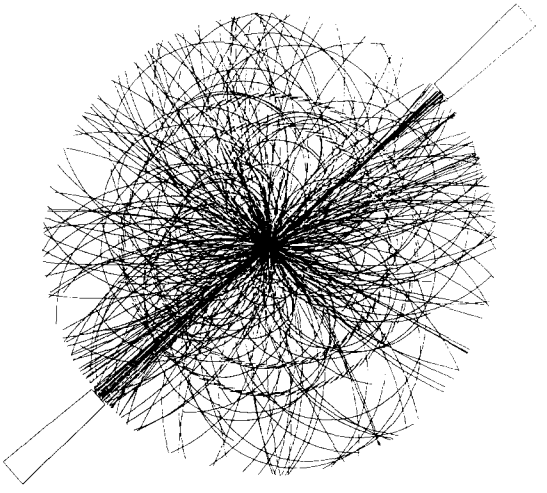

Fig. 14. High-P_T event in a 3 T field.

with a precision given by $\sqrt{2}\,\sigma_m/\delta$. Linking can be done if this accuracy is adequate. In fig. 12 we show the trajectories of two very-high-momentum tracks separated by a production angle of $\langle\theta\rangle$. An incorrect link yields the dashed track whose angles do not match by an amount $\langle\theta\rangle$. Thus, a goal for the linking to work is $\sqrt{2}\,\sigma_m/\delta \lesssim \langle\theta\rangle$. This provides the motivation for a large δ.

Note that a certain number of ambiguities can be tolerated since they can be solved using the information from several layers. However, in order to find tracks with a small number of layers and to keep the number of wrong associations small, $\sqrt{2}\,\sigma_m/\delta \lesssim \langle\theta\rangle$ is a reasonable criterion.

For $\sigma_m = 5$ μm and $\delta = 1$ cm, we get $\sigma_m/\delta = 0.5$ mrad, which is $\sim \langle\theta\rangle$. We will see below, using a full Monte Carlo simulation, that $\delta = 1$ cm is indeed close to optimum.

3.2.2. Effect of tracks with impact parameters

In the above we have assumed that tracks come from the origin when we match the two hits into a vector segment (but not in the vector segment linking). In fig. 13 we show what happens for a track with an impact parameter b.

The displacement of the second hit in a closely spaced pair of detectors at radius r_i, for a very stiff track with impact parameter b with respect to a straight line through the origin, is $d = b\delta/r_i$. For the decay of D

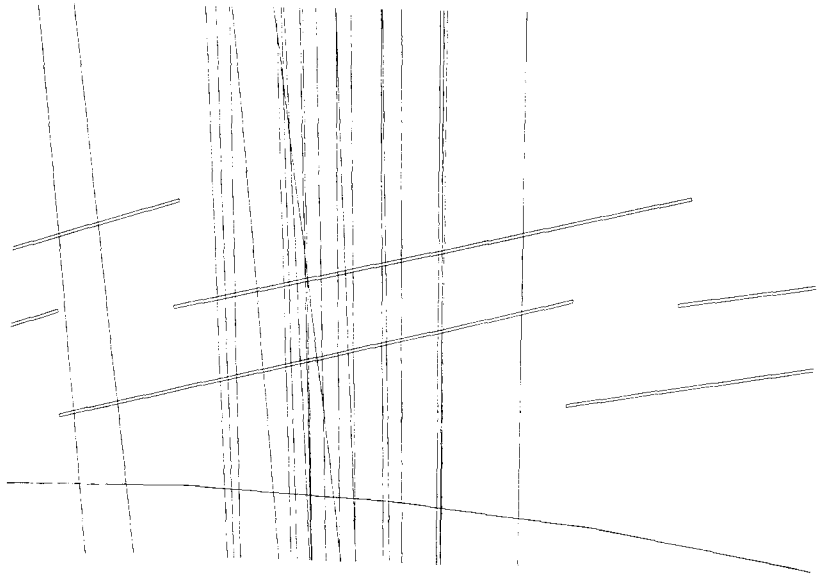

Fig. 15. Blowup of the high-P_T event of fig. 14 showing the jet core.

or B mesons, $b \lesssim 300$ μm. To avoid errors in association for pairs, we require as before $d = b\delta/r_i < r_i\langle\theta\rangle$ or $b < r_i^2\langle\theta\rangle/\delta$. Taking $\delta = 1$ cm and $r_i > 8$ cm implies that there is no problem for $b < 320$ μm, even for the innermost layer. There is a problem for K_S^0, which might have to be picked up in a second pass, if they are close to the jet axis.

3.3. Monte Carlo studies

We have looked in more detail at the ability to do tracking in 1 TeV jets with a silicon tracker. The program ISAJET was used to generate events with two quark or gluon jets, each with $P_T \geq 1$ TeV. The main multiplicity within $|Y| < 2$ in these events is 330, of which 118 have $P_T \geq 1$ GeV. Fig. 14 shows a high-P_T event in a 3 T magnetic field. A region near the core of the tight 1.5 TeV jet in the lower left quadrant of the event, at a radius of 26 cm, has been blown up and is shown in fig. 15. The scale is matched to the size of a single strip detector containing 1024 25 μm elements. (Note that the strips have been tilted to compensate for the Lorentz angle due to the magnetic field.) At this scale, which is the one relevant to the track finding, the stiff tracks are not confusing.

3.3.1. Vector segment finding

To quantify this further, we have performed the first two steps of the pattern recognition for events with 1 TeV jets. As a first step, we keep only hits with no other hit within 100 μm in space. Second, we consider pairs of hits entering the appropriate combination of detectors of 10 cm length in z (we arrange the outer layer of the pair to have detectors staggered by one half of a detector length with respect to the inner layer). Then, using the simple algorithm presented above to link hits into vector segments and considering only hit pairs which can come from tracks with $P_T > 1$ GeV, we evaluate the efficiency vs P_T for finding tracks, requiring at least NVEC = 4, 6 or 8 correctly found vector segments to call the track found. The results for δ chosen equal to 1 or 2 cm are shown in Figs. 16a and 16b, respectively, where the last bin includes overflows. The efficiency approaches 100% for high-momentum

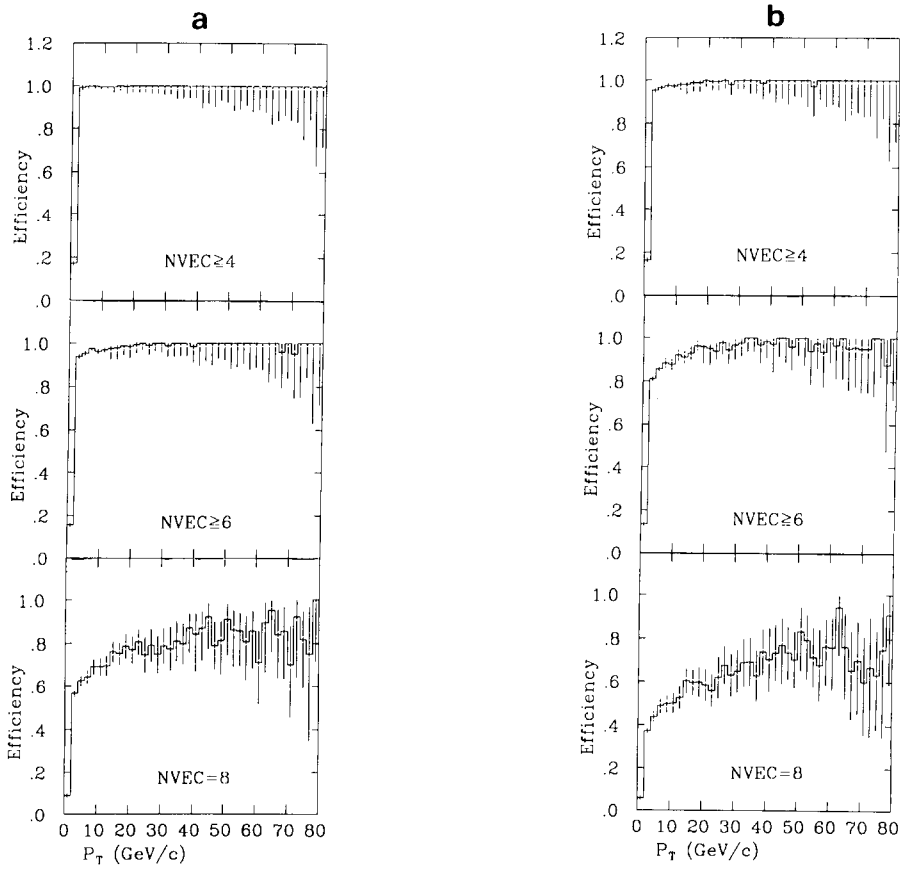

Fig. 16. Tracking efficiency vs P_T as a function of the number of segments reconstructed. (a) $\delta = 1$ cm; (b) $\delta = 2$ cm. The error bars are 95% confidence level limits, from the statistics of the Monte Carlo run.

tracks. In contrast to conventional drift chamber trackers, which are most efficient for low-P_T tracks which separate from jets, the silicon tracker we describe is most efficient for the high-P_T tracks in the core of jets. The figure also indicates that a $\delta = 2$ cm is noticeably worse than $\delta \simeq 1$ cm. Choosing $\delta = 5$ mm would give about a 10% increase in efficiency if all 8 segments are required and little change for the case of 6 or 4 segments found.

3.3.2. Vector segment linking

Once vector segments are found, they must be unambiguously linked together to form tracks. One way to do this is to use a technique employed successfully with the Mark II jet-cell central drift chamber at the SLC [13]. The idea is to calculate the curvature [$\kappa = 1/2\rho_{\text{track}}$] and azimuth at the origin ϕ_0 of a track passing through the origin, and the tangent to the vector segment. A vector segment provides a measure, at average radius $\bar{r}$, of the track azimuth $\bar{\phi}$ and of the rate of change of the azimuth, $\mathrm{d}\phi/\mathrm{d}r$. We thus calculate

$$\kappa = -\frac{\mathrm{d}\phi}{\mathrm{d}r} \Big/ \sqrt{1 + \left(\frac{\bar{r}\,\mathrm{d}\phi}{\mathrm{d}r}\right)^2},$$

$$\phi_0 = \bar{\phi} + \arcsin \kappa \bar{r}.$$

This will produce a mapping in which all vector segments found for a given track should lie near one point in the κ–ϕ_0 plane. The vector segments found for the event shown in fig. 14 have been plotted in fig. 17a. Up to eight vector segments are plotted for each track. One can immediately see the two jets in the event. The effect of resolution in the curvature is also seen from the spread in points for each track. For this plot we have used $\sigma_m = 5$ μm and $\delta = 5$ mm.

Fig. 17b is a blowup of the region around the jet at $\phi_0 \simeq 3.9$ rad. The effect of resolution is now more obvious, and it is also clear that the error in κ is strongly correlated with the error in ϕ_0. This can be parameterized by a 2×2 error matrix, which can be used to cluster the vector segments into tracks. Even by eye, it can be seen from fig. 17b that vector segments from nearby tracks in the jet are becoming confused. This can be remedied by making the paired-layer separation δ larger. The result is shown in fig. 17c, where the improved vector segment resolution obtained by increasing δ from 5 to 10 mm results in clearly separated tracks within the jet. Note that the spread in measured ϕ_0 values is $\sqrt{2}\,\sigma_m/\delta$, the parameter introduced earlier to quantify the ability to link vector segments. After looking at plots for many events with 1 TeV jets, it becomes clear that 1 cm is a good choice for δ and will usually allow vector segment linking for the tracks in the jet core.

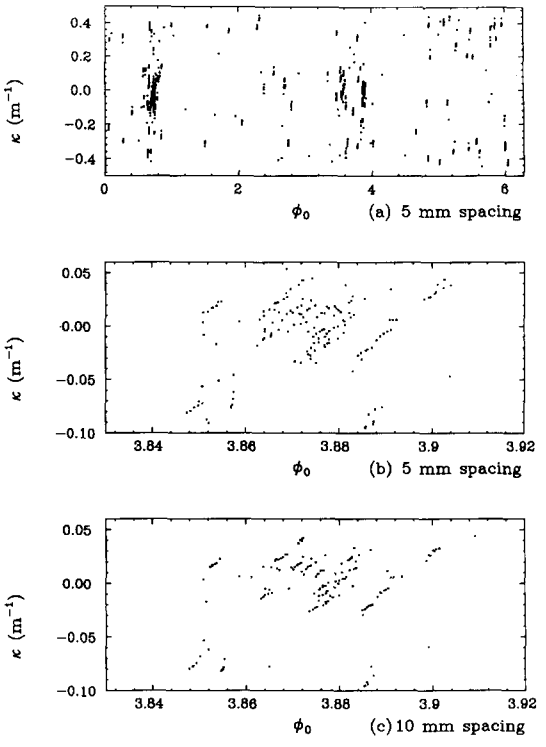

Fig. 17. Plot of κ vs ϕ_0 for vector segments found in the event in fig. 14. Up to eight vector segments per track, and vector segments found incorrectly are also shown. (a) The entire event. (b) Blowup of one of the 1.5 TeV jets, $\delta = 5$ mm. (c) Same as (b), but $\delta = 10$ mm.

3.3.3. Dependence of efficiency on magnetic field

The presence of an axial magnetic field is required for the measurement of the curvature, and hence momentum, of the tracks. This is quantified in section 4, but for now we note that the momentum resolution varies inversely with the magnetic field, making it desirable to have the largest field possible. However, the magnetic field also has an impact on the pattern recognition efficiency. The field may improve the reconstruction efficiency by separating closely spaced tracks in the outer layers, or degrade the efficiency by causing tracks to cross in the outer layers, leading to confusion.

In order to determine which is the dominant effect of the field on pattern recognition for the tracking system discussed here, we evaluated the vector segment finding efficiency for three values of the field, $B = 0$, 2.5 and 5 T. We find that the vector segment finding efficiency is degraded with larger magnetic fields, over the entire range of momenta. The efficiency for finding all eight vector segments for tracks with $P_T > 15$ GeV/c averages $> 95\%$ for $B = 0$, falling to $\simeq 80\%$ and $\simeq 65\%$ for $B = 2.5$ and 5.0 T, respectively.

It appears that, whether the tracks are relatively isolated in the periphery or in the core of a jet, the dominant effect of the magnetic field is to cause tracks to cross, leading to confusion and inefficiency. It is therefore desirable to have the lowest possible magnetic field to obtain the needed momentum resolution; in section 4 we conclude that $B = 2.5$ T is a good choice. With that field, the inefficiency for vector segment finding in the inner layers, due to the close spacing of tracks, is approximately the same as that in the outer layers, due to track crossings.

The magnetic field can also degrade the double-track resolution by spreading the charge (electrons and holes) over several strips, due to the Lorentz drift of the charges in the magnetic field. This effect can be reduced by orienting the detector elements so that their normal vector makes an angle θ_L with respect to the xy-radius vector. The Lorentz angle θ_L is defined by $\tan\theta_L = \mu B$, where μ is the Hall mobility of the charge. However, the use of double-sided detectors (as discussed below) means that we are collecting the charge from both electron and holes, which have different Hall mobilities [14] [$\mu_e \approx 0.15$ m^2/(V s), $\mu_h \approx 0.03$ m^2/(V s)]. To minimize the problem, we can orient the detectors at an angle which is the average of the Lorentz angles for each charge, and choose a magnetic field which is low enough so that the residual Lorentz drift spreads the charge over a strip width or less. A detector of 150 μm thickness in a 2.5 T field oriented at $\tan\theta_L = (\mu_e + \mu_h)B/2$ will spread the charge by 22.7 μm on either side of the detector, just less than one strip width; thus the impact on the double-track separation will be small. Larger magnetic fields will only exacerbate the problem.

3.4. z-measurement

The optimum way to measure the z-coordinate is a complicated question. We look at the use of stereo measurements. Since each strip detector is double-sided, we orient the strips on one side of the detector at a small angle (the stereo angle α) with respect to the axial direction. For detectors of length $l = 10$ cm, a stereo angle of $\alpha = 5$ mrad yields a "stereo displacement" $s = l\alpha = 500$ μm, as illustrated in fig. 18. We assume that each pair of strips is organized as shown in fig. 19, with u stereo strips on one detector of a pair and v stereo strips on the other ($\alpha_u = -\alpha_v$).

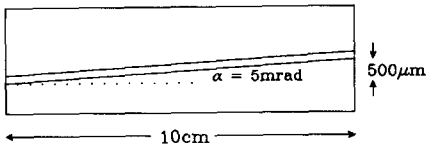

Fig. 18. Stereo displacement of 500 μm over 10 cm for stereo strips.

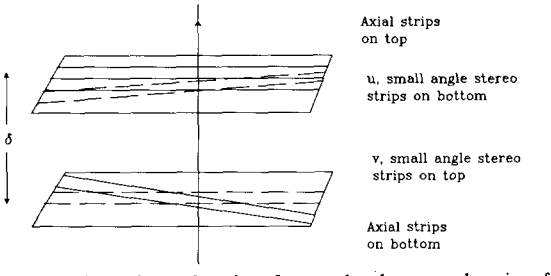

Fig. 19. Orientation of strips for a closely spaced pair of detectors.

The goal for the pattern recognition is to measure z-coordinates locally within each pair. Each of the eight pairs making up the full detector would then have space coordinates and tangent vectors assigned locally to each track. These would then have to be matched from layer to layer, as discussed above.

Tracks separated by more than the stereo displacement s in the axial projection do not interfere with each other at all. A value of $s = 500$ μm is probably small enough to guarantee that most stereo hits can be associated by selecting from a small number of alternative assignments.

The local matching problem in z can come from two tracks which can be confused or from many tracks causing accidental matches. We consider the former case first.

We assume we have two tracks with azimuthal angular coordinates in the layer pair of ϕ_1, ϕ_2 and ϕ_1', ϕ_2'. Then the two stereo measurements in each layer would be:

$$\phi_v = \phi_1 + \frac{\alpha z_1}{r_1}, \quad \phi_v' = \phi_1' + \frac{\alpha z_1'}{r_1};$$

$$\phi_u = \phi_2 - \frac{\alpha z_2}{r_2}, \quad \phi_u' = \phi_2' - \frac{\alpha z_2'}{r_2}.$$

For high-momentum tracks, $z_i = r_i \tan\lambda + z_0$, where z_0 is the vertex position and $\tan\lambda = P_z/P_T$. The correct matches are then found to be the pairs that best satisfy:

$$\phi_1 + \phi_2 = \phi_u + \phi_v, \quad \phi_1' + \phi_2' = \phi_u' + \phi_v',$$

where we take $z_0 = 0$. The full $\sigma_m = 5$ μm precision of the device is available to do the matching. For exactly two correct hits per layer the pairing is therefore relatively easy.

At the SSC we expect the length of the interaction region to be $\sigma_{z_0} \simeq 5$ cm. Assuming complete ignorance of the vertex position in a given event (taking $z_0 = 0$), such a spread in vertex position will produce a mismatch in the angles in the above matching equations of $\sigma_{z_0}\alpha\delta/r^2$. For the detector discussed here this error is larger than the measurement error $2\sigma_m/r$ for $r < 25$ cm and will therefore dominate the error in z-matching at smaller radii.

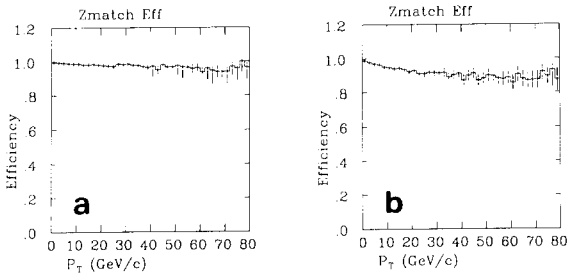

Fig. 20. Efficiency vs P_T for correctly matching the z-strip s in a vector segment found correctly in ϕ. (a) $\alpha = 5$ mrad, (b) $\alpha = 20$ mrad.

In general, we can minimize the z-matching confusion by taking a very small stereo angle α, trading off resolution in z. This does not significantly degrade the momentum or mass resolution for a solenoidal field. In addition, we only need 1 mm resolution in z at the vertex to separate most multiple interactions. The very good 5 μm resolution of the strips, giving $\sigma_z = 1.4$ mm for $\alpha = 5$ mrad, will yield a resolution in z at the vertex of 835 μm.

The confusion from many tracks can be quantified in terms of the detector and physics parameters. Recall that within a jet the mean displacement between tracks at a radius r is $r\langle\theta\rangle$. If a pair of axial strips has been successfully associated within the jet, all tracks within the stereo displacement region s (defined above) will leave stereo hits which can confuse the z-matching. The number of tracks entering this region is $N_s = s/(r\langle\theta\rangle)$. All of these tracks will leave stereo hits in the u-plane which could accidentally associate with another hit in the v-plane falling within a region of full width $2\sigma_m$, which is the resolution characterizing the correct choice. The probability of there being such a hit in the v-plane is therefore $\mathcal{P} = N_s \cdot 2\sigma_m/s$, and the number of potential incorrect z pairings is $N_{\text{inc.}z} = N_s\mathcal{P}$. Thus we arrive at the scaling rule for stereo association to work well:

$$N_{\text{inc.}z} = N_s^2 \frac{2\sigma_m}{s} = \frac{2\sigma_m s}{(r\langle\theta\rangle)^2} < 1.$$

For the detector considered above, $N_{\text{inc.}z} \simeq 0.5$ at a

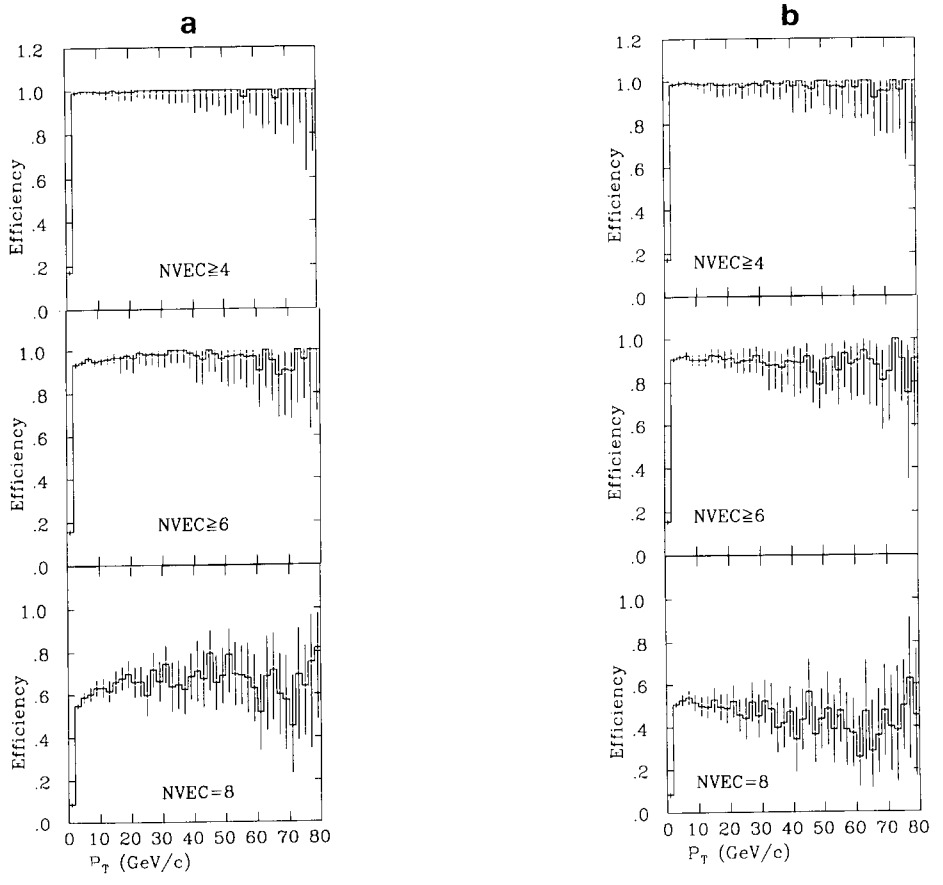

Fig. 21. Tracking efficiency vs P_T as a function of the number of segments reconstructed in ϕ *and* z. (a) $\delta = 1$ cm, $\alpha = 5$ mrad; (b) $\delta = 1$ cm, $\alpha = 20$ mrad.

radius of 20 cm. Thus, at larger radii, it may be possible to use longer detectors (e.g. bonding two or three 10 cm long detectors together) in order to minimize the number of electronics channels required.

Note that if we increase s (by increasing the stereo angle α or the detector length l), $N_{\mathrm{inc}.z}$ will not necessarily continue to increase. Eventually s will exceed the size of the jet ($\simeq 2r\theta_{1/2}$) and any further increase in s will leave $N_{\mathrm{inc}.z}$ unchanged. Taking $\theta_{1/2} = 10$ mrad and $s = 500$ μm, we find that the stereo displacement encompasses the entire jet when $r < 2.5$ cm. At smaller radii our scaling rule gives

$$N_{\mathrm{inc.}\ z} = \frac{4\sigma_{\mathrm{m}} r\theta_{1/2}}{(r\langle\theta\rangle)^2} = \frac{2\sigma_{\mathrm{m}}}{(r\langle\theta\rangle)} \frac{2\theta_{1/2}}{\langle\theta\rangle} = \frac{4\theta_{1/2}\sigma_{\mathrm{m}}}{r\langle\theta\rangle^2} < 1.$$

This is never the case for the detector configuration proposed here, but is relevant for other detector configurations such as large drift chambers.

Finally, we note that the added information about the dip angle (tan λ) of a track producing the vector segment will not help in vector segment linking, due to the relatively poor resolution in the dip angle as compared to the azimuthal angle measurement.

3.4.1. z-matching in the Monte Carlo study

In order to test our scaling rule for z-matching, we use the same events containing 1 TeV jets as were used in section 3.3 above, where the finite beam length with $\sigma_{z_0} = 5$ cm is included. We apply the z-matching algorithm above to vector segments that were found correctly in the axial projection. The efficiency for making the correct z-match is shown in figs. 20a and b as a function of P_T of the track, for the cases $\alpha = 5$ and 20 mrad, respectively. In the former case the efficiency is $> 95\%$ for all tracks, falling at high P_T where tracks are in the center of jets. It is clear that the efficiency begins to degrade significantly when the stereo angle is increased to 20 mrad, as predicted by our scaling rule, and we have verified that the effect continues at larger stereo angles.

We can combine the requirements of correct matching in ϕ and in z by plotting the efficiency vs P_T for finding tracks, if we require at least 4, 6 or 8 vector segments correctly found in ϕ *and* z to call the track found. This is shown in figs. 21a and b for the cases $\alpha = 5$ and 20 mrad, respectively, where in both cases $\delta = 1$ cm. We conclude that choosing $\delta = 1$ cm, $\alpha = 5$ mrad provides a good match to the physics demands at 1 TeV.

4. Momentum resolution

We look at the expected momentum resolution for the silicon tracker discussed above. We will assume a vertex-constrained fit as would be appropriate for the high-momentum leptons from the heavy-Higgs decay. For high momentum the orbit equations for a circle are:

$$\phi = \phi_0 + \frac{r}{2\rho_{\mathrm{track}}}, \quad z = r\ \tan\ \lambda + z_0,$$

where the track parameters are: ϕ_0, ρ_{track}, tan λ and z_0. Measuring the track angles ϕ at m radii r_1, r_2, $\cdots r_m$, the values of ϕ_0 and ρ_{track} are extracted by minimizing

$$\chi^2 = \sum_{i=1}^{m} \frac{(r_i\phi_i - d_i)^2}{\phi_i^2},$$

where d_i is the measured circumferential distance for the ith axial layer. The expected error in d_i is σ_i.

Relating ρ_{track} to P_T and calculating the errors from the χ^2 gives a result

$$\frac{\sigma_{P_T}}{P_T^2} = \frac{2}{0.3B} \sqrt{\frac{\sum_{i=1}^{m} \frac{r_i^2}{\sigma_i^2}}{\sum_{i=1}^{m} \frac{r_i^2}{\sigma_i^2} \sum_{i=1}^{m} \frac{r_i^4}{\sigma_i^2} - \left(\sum_{i=1}^{m} \frac{r_i^3}{\sigma_i^2}\right)^2}},$$

where B is in Tesla, P_T in GeV and all distances are in meters.

Assuming that the four measurements in a superlayer give an effective measurement with an error σ, and that the eight superlayers are approximately equally spaced out to a maximum radius r_m, gives, after performing the sums above:

$$\frac{\sigma_{P_T}}{P_T^2} = \frac{5.5\sigma}{0.3Br_m^2}.$$

Taking $\sigma = 3$ μm, after averaging over the four measurements in a superlayer, and $r_m = 0.5$ m gives:

$$\frac{\sigma_{P_T}}{P_T^2} = \frac{6.5\%}{0.3B}\ [\mathrm{TeV}^{-1}].$$

Thus, a field of 4 T would give $\sigma_{P_T}/P_T = 5.5\%$ of P_T [TeV], while a field of 2.5 T would give $\sigma_{P_T}/P_T = 8.8\%$ of P_T [TeV].

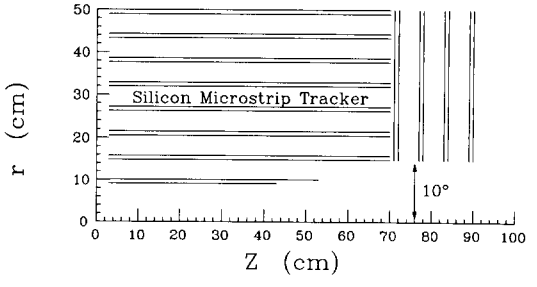

Fig. 22. Plan of the silicon tracking system, with azimuthal symmetry.

For the intermediate-mass Higgs search, as discussed earlier, we wish to reconstruct Z^0 masses using leptons with a resolution better than the natural width limit which implies that we want $\sigma_{P_T}/P_T \lesssim 2\%$ at about 200 GeV. Thus, a field $B \gtrsim 2.5$ T would be adequate. Since we want to minimize the tracking inefficiency and the Lorentz angle for electron motion in the silicon, 2.5 T is probably an optimum choice for the field.

For such good resolution the multiple-scattering contribution to the resolution will dominate up to rather high momentum. Assuming 4–5% of a radiation length and a 50 cm path length the multiple-scattering contribution is approximately $\sigma_{P_T}/P_T = 0.8\%$ for $B = 2.5$ T. This value is comparable to the value typical of present-day central drift chamber systems.

Fig. 22 shows a possible arrangement for the tracking detector in r vs z, having azimuthal symmetry. It contains about 40 m^2 of silicon detectors. Going out in θ, this arrangement gives:

(a) tracking with ≥ 6 superlayers for $170^0 \geq \theta \geq 10^0 (|Y| \leq 2.3)$;
(b) tracking with 8 superlayers for $160^0 \geq \theta \geq 20^0 (|Y| \leq 1.75)$;
(c) tracking over a fixed radius of 50 cm for $154^0 \geq \theta \geq 26^0 (|Y| \leq 1.44)$;
(d) tracking with axial strips for $143^0 \geq \theta \geq 37^0 (|Y| \leq 1.10)$.

Assuming $\sigma_{P_T}/P_T = 8\%$ of P_T [TeV] at 90^0 and ignoring multiple scattering, fig. 23 shows σ_P/P^2 vs rapidity, for P in TeV.

The use of silicon, combined with a moderately large magnetic field, allows very good resolution. It is essential, however, to align the silicon to an accuracy of a few μm in order to achieve this resolution in practice.

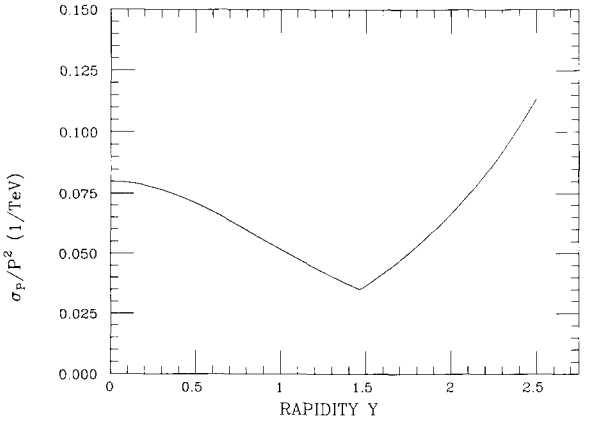

Fig. 23. Momentum resolution vs rapidity for the silicon tracking system.

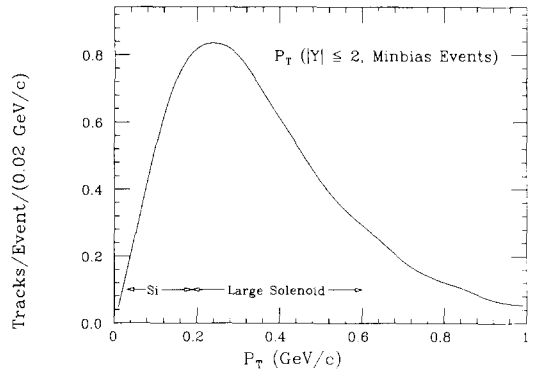

Fig. 24. Transverse-momentum spectrum for minimum bias events. The ranges indicated by arrows are described in the text.

5. Spiraling tracks and photon conversions

The presence of a large magnetic field tends to trap particles in the field increasing the occupancy and radiation damage. In this section we look at this problem as a function of the B field, tracker radius and rapidity coverage.

Fig. 24 shows the momentum spectrum from ISAJET for minimum bias events. A track will be trapped in the field for $2\rho_{\text{track}} \leq r_m$. Thus, for example, trapping will occur for $P_T \leq 190$ MeV at $r_m = 50$ cm, $B = 2.5$ T, for a compact solenoid; or $P_T \leq 600$ MeV at $r_m = 160$ cm, $B = 2.5$ T, for a large solenoidal detector. A large fraction of the tracks in minimum bias events occurs in this momentum range, so trapping can be important. The ranges for trapping are indicated in fig. 24 for the two detector configurations with 2.5 T fields.

To estimate the effect we have calculated the effective track length seen in the detector per minimum bias event using the ISAJET MINBIAS model (note that it gives $\simeq 5.1$ charged tracks per unit rapidity at SSC energies, which may be a significant underestimate). We have looked at both a compact and a large solenoid [15]. The dimensions for each tracking system have been taken to be $r_{\text{inner}} = 8$ cm, $r_{\text{outer}} = 50$ cm and $r_{\text{inner}} = 50$ cm, $r_{\text{outer}} = 160$ cm, respectively. Tracks passing through a part of the detector only (for $2\rho_{\text{track}} < r_{\text{outer}}$, or exiting in z in the middle of a spiral) are counted as fractions. Tracks with $2\rho_{\text{track}} < r_{\text{inner}}$ make no contribution. The maximum number of spirals allowed is 100, based on estimates of energy loss and multiple scattering. We have repeated the calculation, with this number reduced to 30, to study the effects of this cutoff. The change in total track length is 20%, which provides an estimate of the uncertainty in the calculation. The results are presented in tables 2 and 3 as a function of the B field and rapidity coverage.

Table 2
Average number of track lengths per minimum bias event for the *compact* solenoid

Y range	B field [T]						
	0	1.5	2.0	2.5	3.0	3.5	4.0
$\|Y\| \leq 1.0$	9.6	11.5	12.6	14.0	15.6	17.4	19.8
$\|Y\| \leq 1.5$	14.8	18.1	20.2	22.9	26.0	29.4	33.5
$\|Y\| \leq 2.0$	20.1	25.6	29.5	34.0	39.4	45.2	52.0
$\|Y\| \leq 2.5$	25.8	34.6	41.2	48.8	58.1	67.5	78.3

Table 3
Average number of track lengths per minimum bias event for the *large* solenoid

Y range	B field [T]						
	0	1.5	2.0	2.5	3.0	3.5	4.0
$\|Y\| \leq 1.0$	9.6	18.2	19.4	18.3	16.1	13.5	11.3
$\|Y\| \leq 1.5$	14.8	31.4	33.2	31.2	27.7	23.5	19.6
$\|Y\| \leq 2.0$	20.1	48.8	52.5	49.5	44.4	37.8	31.4
$\|Y\| \leq 2.5$	25.8	74.1	80.2	76.1	68.4	58.6	48.6

From the tables we see that for both detectors at $B = 2.5$ T the occupancy is increased by as much as a factor of 2 or more, as compared to $B = 0$. For the compact solenoid the occupancy is not a problem because of the large segmentation and excellent time resolution. Silicon detectors are able to resolve the hits from every beam crossing separately. Even at the innermost radius of 8 cm, with a luminosity of 10^{33}, the occupancy is $\sim 2 \times 10^{-3}$ in a two- hit resolution element = 100 μm (4 strips) of 10 cm length. This contrasts with an occupancy of about 20%, at a 50 cm radius, for a 4 mm diameter cell in a large solenoidal

Table 4
Detector parameters and scaling rules

Physics parameters for	1 TeV jets		50 GeV jets
Track angular separation $\langle\theta\rangle$	0.5 mrad		10 mrad
Jet angular width $\theta_{1/2}$	10 mrad		40 mrad
Track P_T in jet core	50 GeV		10 GeV
Detector Parameters	**Si tracker**	**Drift chamber**	**Mark II/SLC**
Magnetic field B [T]	2.5	2.5	0.5
Radius of curvature $\rho = 3.3\ P_T/B$ [m]	66	66	66
Radial detector spacing δ [cm]	1	1	0.8
Superlayer thickness δ_{SL} [cm]	1	4	4
Maximum radius r_m [cm]	50	160	150
Mean radius r [cm]	29	100	88
Detector length l [cm]	10	>100	230
Double track separation ϵ_m [mm]	0.1	3	4
Stereo angle α [mrad]	5	50	74
Position resolution σ_m [μm]	5	100	100
z-position resolution $\sigma_z = \sqrt{2}\,\sigma_m/\alpha$ [mm]	1.4	2.8	1.9
Scaling-rule requirements	**Si tracker**	**Drift chamber**	**Mark II/SLC**
Resolve hits: $\epsilon_m/r\langle\theta\rangle < 1$	0.7	6.0	0.45
Find vector segments: $\delta/(2\rho\langle\theta\rangle) < 1$	0.15	0.15	0.006
Link vector segments: $\sqrt{2}\,\sigma_m/(\delta_{SL}\langle\theta\rangle) < 1$	1.4	7.1	0.4
Match z hits: $2\sigma_m l\alpha/(r\langle\theta\rangle)^2 < 1$, or:	0.24	–	–
for $l\alpha > 2r\theta_{1/2}$: $4\sigma_m\theta_{1/2}/(r\langle\theta\rangle^2) < 1$	–	16.0	0.2

detector covering $|Y| \leq 1.5$, assuming a pileup of only 4.8 events (3 beam crossings). In the central rapidity region $|Y| \leq 1.0$, containing the silicon strips nearest to the beam in fig. 22, the spiraling tracks would increase the occupancy and radiation damage by 40% for a 2.5 T B field. The radiation damage issue would argue for the smallest magnetic field consistent with the physics goals of the detector.

Finally, we consider the effect of photon conversions in the tracking system. This will be a serious problem for a detector with a substantial fraction of a radiation length of material. The converted electron spectrum is very soft since each π^0 decays into two photons and each photon converts into two particles) the π^0 momentum spectrum is taken to be the same as charged primaries, fig. 24). We assume that, because the conversion electrons are so soft, they all spiral in the detector for nearly any radius of conversion. There are roughly half as many π^0s as charged particles, giving $2X_0$ converted electrons per primary charged track, where X_0 is the amount of material in the tracking system in radiation lengths. From tables 2 and 3 we estimate the number of track lengths per spiralling track, $r \simeq 4$ for both detector configurations. Also from tables 2 and 3 we read off the number of track lengths for $B = 0$, N_0, and the number for $B = 2.5$ T, $N_{2.5}$. We then obtain, for both the compact and large solenoid,

$$\frac{\text{Track length due to conversions}}{\text{Track length due to primary charged tracks}} \simeq \frac{2X_0N_0r}{N_{2.5}}.$$

This gives $\simeq 4X_0$ for both detector configurations. Clearly a value of $X_0 \leqslant 5\%$ is very desirable. Note that the 20% occupancy for the large solenoid detector, with $X_0 = 8\%$ [15], will increase to 26% due to photon conversions.

6. Conclusions

A tracking system capable of reconstructing charged-particle tracks in 1 TeV jets at the LHC or SSC will be a powerful tool for identifying decays of the Higgs boson, in low-multiplicity modes containing leptons, in modes containing b jets and in high-multiplicity hadronic modes. Very precise momentum measurements will aid in identifying $Z^0 \to l^+l^-$ decays. Impact parameter measurements will allow tagging of b jets. Multiplicity cuts can be used to identify $W \to q\bar{q}$ decays despite a very large QCD background.

We have specified the requirements for such a tracking system, emphasizing the tradeoffs in achieving optimal pattern recognition. We have proposed a design, using silicon microstrips, which can meet the design requirements. The outer radius of this detector is 50 cm and the magnetic field needed is 2.5 T.

Using simple scaling rules relating the physics and detector parameters, we can evaluate the ability of such a system to perform efficient pattern recognition in the core of 1 TeV jets. These parameters and scaling rules are summarized in table 4. In that table we also summarize typical design parameters for SSC drift chamber tracking systems [15], and for the Mark II upgrade central drift chamber [16] at the SLC. Numerous Monte Carlo simulations [17] have verified that the Mark II drift chamber is well suited to the track densities expected at the SLC, but its performance begins to degrade when some detector parameters (most notably ϵ_m) are made less favorable. From the table it is clear that the proposed silicon tracker system is quite capable of reconstructing tracks in 1 TeV jets, while typical SSC drift chamber designs will have serious problems due to the relatively poor position resolution (most especially in resolving closely spaced hits and performing axial and stereo vector segment linking).

Monte Carlo studies of the silicon tracker pattern recognition efficiency confirm that efficient track reconstruction is possible even in the core of 1 TeV jets. The expected momentum resolution for such a tracking system is sufficient to reconstruct Z^0 masses in $\mu^+\mu^-$ final states with a resolution better than the natural width for parent Higgs masses up to ~ 1 TeV.

Lastly, we point out that spiraling tracks from primary charged particles and photon conversions, which can produce a significant occupancy in large drift chamber/solenoid detectors, are of no concern for a compact silicon tracking system.

References

[1] J. Kirkby et al., Proc. Workshop on Experiments, Detectors, and Experimental Areas for the Supercollider, Berkeley, 1987, p. 388.
[2] B. Cox et al., 1986 Summer Study on the Physics of the SSC, Snowmass, Colorado, p. 33.
[3] J. Brau, L. Price, G. Kane et al., Proc. Workshop on Experiments, Detectors, and Experimental Areas for the Supercollider, Berkeley, 1987, p. 728.
[4] J. Brau, private communication (1987).
[5] F.E. Paige and S.D. Protopopescu, ISAJET 5.34.
[6] S.D. Protopopescu, 1986 Summer Study on the Physics of the SSC, Snowmass, Colorado, p. 180.
[7] H.-U. Bengtsson and T. Sjoestrand, PYTHIA 4.8, UCLA-87-001.
[8] For some aspects of B meson detection, see B. Cox et al., SLAC-PUB-4144; and F.J. Gilman and L.E. Price, SLAC-PUB-4138.
[9] Proc. ECFA-CERN Workshop on a Large Hadron Collider in the LEP Tunnel, Lausanne and Geneva, March, 1984 (CERN 84-10, 1984), P. Jenna et al., p. 200 and A. Al et al., p. 503.

[10] K. Hayes, B-Tagging at the SLC, SLAC Mark II/SLC Internal Note no. 73 (1984).
[11] Report of the Task Force on Detector R&D for the Superconducting Super Collider, SSC-5R-1021 (June 1986).
[12] W. Atwood, SLAC SLD experiment, Internal Note no. 135.
[13] J. Perl et al., Nucl. Instr. and Meth. A252 (1986) 616.
[14] E. Belau et al., Nucl. Instr. and Meth. 214 (1983) 253; and R. Horisberger, private communication.
[15] G.G. Hanson et al., Report of the Large Solenoid Detector Group, Proc. Workshop on Experiments, Detectors, and Experimental Areas for the Supercollider, Berkeley, 1987, p. 340.
[16] A.J. Weinstein, Performance of the New Central Drift Chamber for the Mark II at SLC, University of California at Santa Cruz Preprint SCIPP-87/78 (1987).
[17] Proc. SLC Workshop on Experimental Use of the SLAC Linear Collider, March 1982 (SLAC-Report-247) p. 143; A.J. Weinstein, SLAC Mark II/SLC Internal Note no. 155 (1986).